

SCIENTIFIC REPORTS



OPEN

Imaging of Endogenous Metabolites of Plant Leaves by Mass Spectrometry Based on Laser Activated Electron Tunneling

Received: 12 October 2014

Accepted: 22 March 2016

Published: 07 April 2016

Lulu Huang*, Xuemei Tang*, Wenyang Zhang, Ruowei Jiang, Disong Chen, Juan Zhang & Hongying Zhong

A new mass spectrometric imaging approach based on laser activated electron tunneling (LAET) was described and applied to analysis of endogenous metabolites of plant leaves. LAET is an electron-directed soft ionization technique. Compressed thin films of semiconductor nanoparticles of bismuth cobalt zinc oxide were placed on the sample plate for proof-of-principle demonstration because they can not only absorb ultraviolet laser but also have high electron mobility. Upon laser irradiation, electrons are excited from valence bands to conduction bands. With appropriate kinetic energies, photoexcited electrons can tunnel away from the barrier and eventually be captured by charge deficient atoms present in neutral molecules. Resultant unpaired electron subsequently initiates specific chemical bond cleavage and generates ions that can be detected in negative ion mode of the mass spectrometer. LAET avoids the co-crystallization process of routinely used organic matrix materials with analyzes in MALDI (matrix assisted-laser desorption ionization) analysis. Thus uneven distribution of crystals with different sizes and shapes as well as background peaks in the low mass range resulting from matrix molecules is eliminated. Advantages of LAET imaging technique include not only improved spatial resolution but also photoelectron capture dissociation which produces predictable fragment ions.

Currently, secondary ion mass spectrometry (SIMS)^{1,2}, matrix-assisted laser desorption ionization (MALDI)³⁻⁵ and desorption electrospray ionization (DESI)⁶⁻⁸ imaging of biological samples have allowed scientists to obtain spatial distributions of a wide range of biological molecules in tissues that are critical for understanding of their physiological roles⁹⁻¹¹. Among these three approaches, SIMS provides the best lateral resolution (~50 nm) so far. It has a long history for biological imaging but suffers from extensive fragmentations due to energetic desorption/ionization and limitations in the efficiency for secondary ion production. In contrast, MALDI is a soft ionization approach where pulsed laser beams are fired at matrix crystals with embedded analyzes. It offers spatial resolution in the level of micrometers which enables applications on the cellular or sub-cellular levels. However, background peaks in low mass region of time of flight (TOF) instrument, as well as serious contamination of ion source chamber resulting from organic matrix molecules limit its application for analysis of small molecules and other biological molecules. Nanostructure-initiator mass spectrometry (NIMS)¹²⁻¹⁴ has recently emerged as an alternative new method for MS imaging that does not need chemical matrix materials. The spatial resolution can be down to 150 nm. In this approach, initiator molecules are trapped in nanostructured surfaces or clathrates to release and ionize intact molecules adsorbed on the surface. Both NIMS and MALDI MS analyze biological samples in the vacuum. DESI is an atmospheric pressure technique that evaporates and ionizes molecules with a fine spray of charged droplets in the open air. It is well established for ambient surface analysis of every kind of samples such as metabolites, proteins, animal tissue sections, luggage screening for explosives as well as latent fingerprints. The major challenge of DESI is the spatial resolution for biological applications. Additionally, in the case of analysis of plants, the surface wax layer and strong cell wall prevent the penetration of the spray of liquid droplets.

Mass Spectrometry Center for Structural Identification of Biological Molecules and Precision Medicine, Key Laboratory of Pesticides and Chemical Biology, Ministry of Education, College of Chemistry, Central China Normal University, Wuhan, Hubei 430079, P. R. China. *These authors contributed equally to this work. Correspondence and requests for materials should be addressed to H.Z. (email: hyzhong@mail.ccnu.edu.cn)

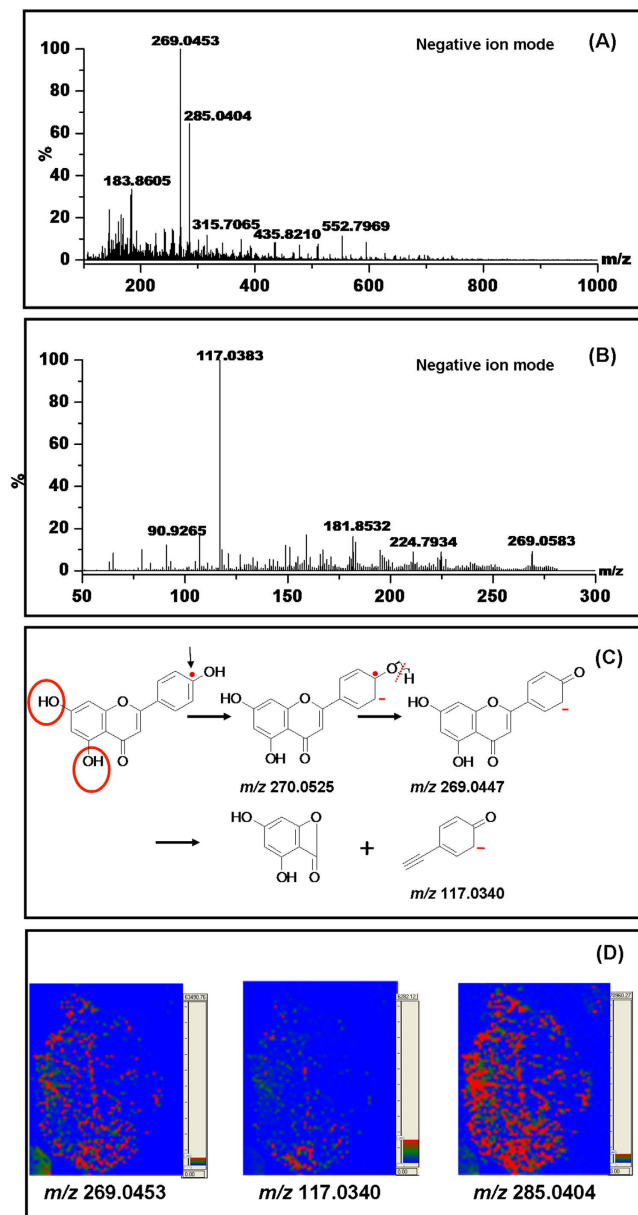


Figure 1. (A) Mass spectrum of the leaf stuck on the surface of bismuth cobalt zinc oxide film; (B) MS/MS spectrum of the selected ion at m/z 269.0453; (C) Illustration of the production of fragment ion at m/z 117.0340; (D) Mass spectrometric imaging of two putatively identified flavone derivatives at m/z 269.0453 and 285.0404 as well as the fragment ion at m/z 117.0340.

We herein describe the new application of a newly developed soft ionization approach based on laser activated electron tunneling (LAET)^{15–17} from semiconductor nanoparticles of bismuth cobalt zinc oxide. These nanoparticles not only can absorb UV irradiation but also have high electron mobility. Although nanoparticles such as gold, titanium dioxide, carbon nanotubes and zinc oxide have been used as inorganic matrix materials for MALDI and SALDI MS (surface assisted laser desorption ionization mass spectrometry) analysis for many years^{18–22}, research efforts have been focused only on their roles as energy mediators. It has been widely accepted that nanoparticles have high surface areas, high photo absorption capabilities and can effectively transfer photo energy to surrounding analyze molecules, which are eventually ionized and detected in positive ion mode of mass spectrometers^{23–25}. This work is aimed to demonstrate the roles of photo-generated electrons in ionization of biological molecules. It is applied as a new avenue for imaging of endogenous metabolites present in plant leaves.

Methods

Reagents and apparatus. LC-MS grade water, acetonitrile (ACN), ethanol and isopropanol were purchased from Fisher Scientific (Bridgewater, NJ, USA). Nanoparticles of bismuth cobalt zinc oxide (Bi_2O_3)_{0.07}(CoO)_{0.03}(ZnO)_{0.9} (<100 nm BET or <50 nm XRD), gibberellic acid (GA), salicylic acid (SA), jasmonic acid (JA),

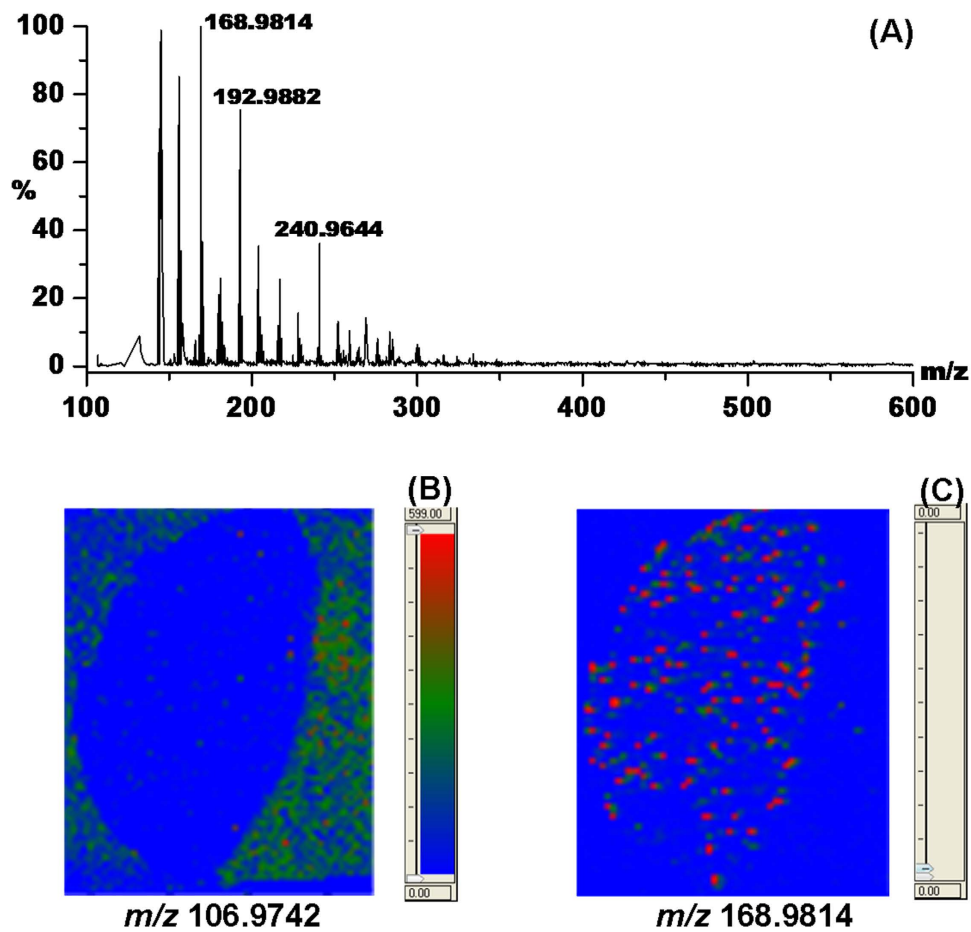


Figure 2. (A) Mass spectrum of the tape-blocked leaf stuck on the surface of bismuth cobalt zinc oxide film; (B) Mass spectrometric imaging of the ion at m/z 106.9742; (C) Mass spectrometric imaging of the ion at m/z 168.9814.

indoleacetic acid (IAA) and abscisic acid (ABA) were purchased from Sigma-Aldrich (St. Louis, MO, USA). Free fatty acids including C6:0, C8:0, C10:0, C12:0, C14:0, C16:0, C18:0, C20:0 and C22:0 were purchased from NU-CHEK PREP, Inc (Elysian, MN, USA) for instrumental calibration. Aluminum tape was purchased from Junke (Shanghai, China).

Preparation of compressed thin films of bismuth cobalt zinc oxide. Nanoparticles of bismuth cobalt zinc oxide (Bi_2O_3)_{0.07}(CoO)_{0.03}(ZnO)_{0.9} were thermally treated at 350 °C for 2 hours in a muffle furnace made by Jianli Furnace Co. Ltd (Yingshan, Hubei, China) before use in order to remove trace organic contaminants. Then about 10 mg of those treated nanoparticles were put on the sticky surface of a single-sided adhesive aluminum tape and compressed under 10 MPa of pressure for 2 minutes by a compressor that is regularly used in infrared spectroscopic analysis. By using this approach, a very uniform and tight flat thin film of bismuth cobalt zinc oxide can be obtained.

Preparation of plant leaves. Freshly obtained plant leaves (*Cayratia japonica*) were tightly pressed onto the top of the thin film of bismuth cobalt zinc oxide. It is very critical for leaves to be tightly attached to the surface of bismuth cobalt zinc oxide. Otherwise, no signals can be obtained. In order to make sure that there is no air gap between the leaf and the flat thin film, the leaf was compressed under 0.1 MPa pressure against the film. Glue tapes were attached to short stems in order to fix the position of the leaves on the film. Then the aluminum tap was finally taped on the sample plate.

Mass spectrometric analysis. A Waters Synapt G2 HDMS system (Billerica, MA, USA) with a MALDI source was used for mass spectrometric imaging. Data acquisition for visualization of spatial distribution of negatively charged molecular ions and fragment ions was obtained through moving the sample plate. The mass spectrometer is equipped with an Nd: YAG high repetition laser head (355 nm). Laser spot size is adjustable from 5 μm to 250 μm . In this work, laser spot size was fixed at \sim 15 μm . Laser influx (355 nm) has been set as 200 units. Laser pulse width is 3 ns and laser fire rate was set as 200 Hz. Pulse energy is 100 $\mu\text{J}/200$ Hz. For each pixel, the acquisition time is 1 second. Potential difference between the sample plate and the aperture were set as 20 volts. Voltages on the sample plate and aperture are 87 volts and 107 volts respectively for this work. In negative ion mode, the instrument was internally calibrated with standard solution of free fatty acids.

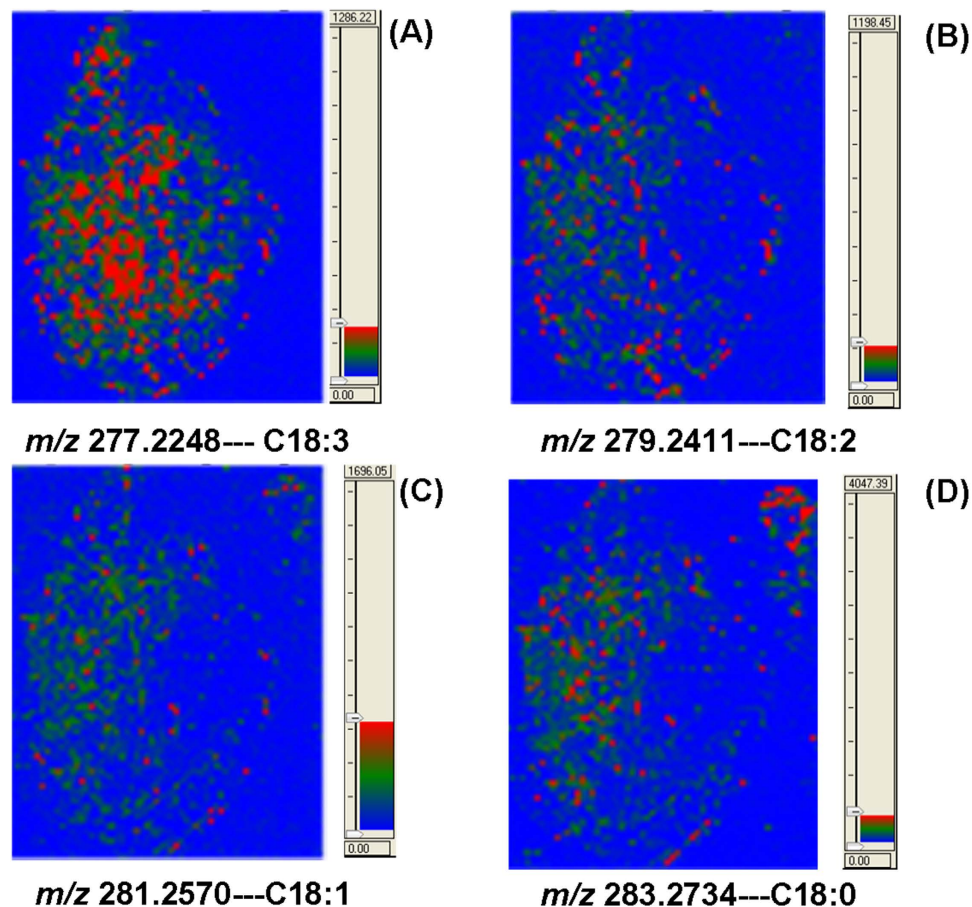


Figure 3. Mass spectrometric imaging of putatively identified long chain fatty acids including C18:3 (A), C18:2 (B), C18:1 (C) and C18:0 (D).

For quantitative assessment of the proposed approach, nanoparticles of semiconductors were suspended in a pure isopropanol solution to reach a concentration of ~ 10 mg/ml and then pipetted into sample wells of the sample plate. Gibberellic acid, salicylic acid, jasmonic acid, indoleacetic acid and abscisic acid were dissolved in a solution containing 50% (v/v) acetonitrile and 50% (v/v) ethanol to reach a concentration of 100 mg/mL. After nanoparticles on the sample plate were air dried, 1 μ L of standard solutions of fatty acids, or samples was deposited on the surface of nanoparticles for downstream mass spectrometric analysis.

For mass spectrometric imaging analysis, the Waters software MALDI Imaging Pattern Creator (Billerica, MA, USA) was used to define the imaging areas before subject to laser shot. The step size of laser beams scanning across the leaf was set as $250 \mu\text{m} \times 250 \mu\text{m}$. Decreased step size improves spatial resolution but it takes longer time to establish the imaging. In the case of leaf analysis, long analysis time may cause dehydration of leaves. Taken together throughput and resolution, the step size of $250 \mu\text{m} \times 250 \mu\text{m}$ was used for all imaging experiments of leaves.

Putative identification of plant endogenous metabolites was achieved by accurate masses and MS/MS fragment ions. As for high abundant molecules, MS/MS experiments have been performed. But only MS experiments have been performed for low abundant molecules. Images of ions have been compared with that of spontaneously generated fragment ions in order to validate the identities of observed ions. Mass spectrometric data have been searched against METLIN database (<http://metlin.scripps.edu>).

Results and Discussion

Principles of LAET ionization, fragmentation and mass spectrometric imaging. As shown in Supplementary Figure 1, nanoparticles of bismuth cobalt zinc oxide were compressed into a uniform thin film under 10 MPa pressure. The thin film is then stuck on the surface of a conductive sample plate. Voltages applied on the sample plate, extraction plate, hexapole and aperture were indicated as V0, V1, V2 and V3 respectively. Upon the irradiation of 355 nm UV laser pulses (3.5 eV, 3 ns width), electrons are excited from valence bands (VB) to conduction bands (CB), leaving holes behind. In negative ion mode of MALDI mass spectrometer, nanoparticles and samples were lined up in the same direction as that of the electric field present in the ion source chamber. Therefore the recombination of electron-hole pairs can be efficiently inhibited because these electrons and holes move in inverse directions and are instantly separated by the external electric field. With appropriate energies, photoexcited electrons can resonantly tunnel away from the surface barrier and eventually captured by charge deficient atoms present in neutral molecules through a nonergodic process. Because the pressure in ion source chamber of the mass spectrometer is usually around 6×10^{-4} mbar, highly reactive oxygen radical ions

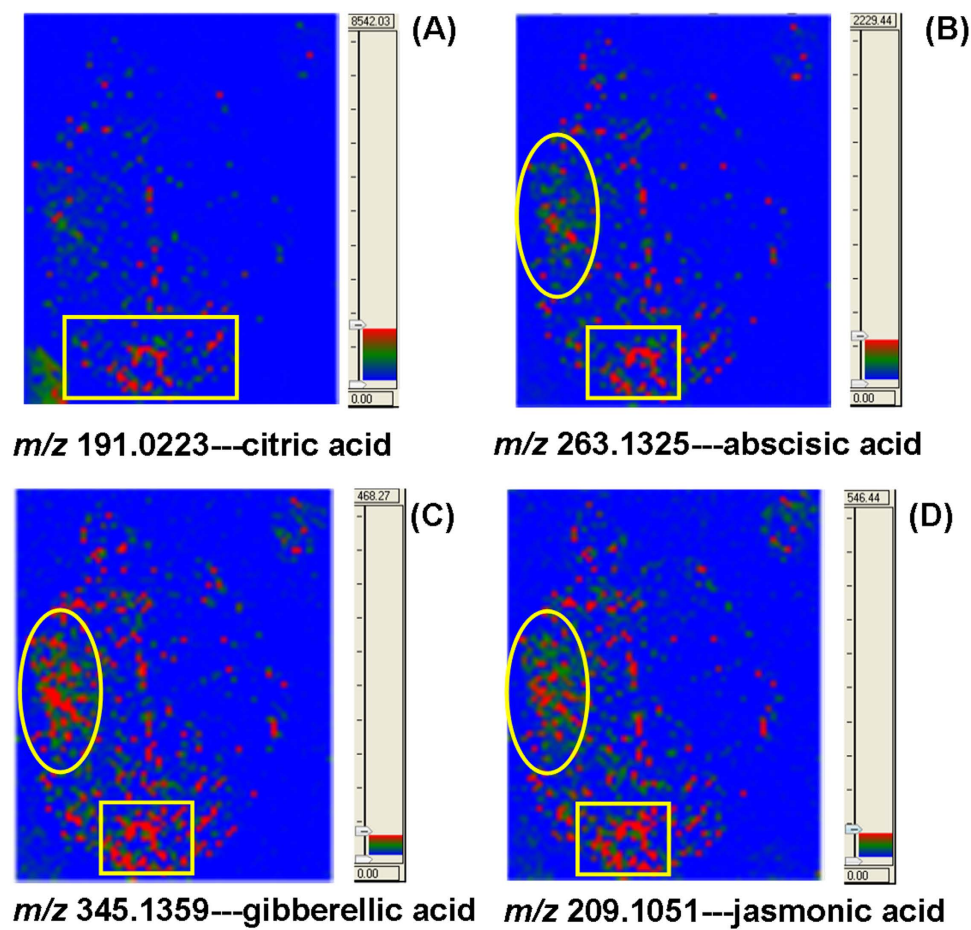


Figure 4. Mass spectrometric imaging of putatively identified small organic acids and phytohormones including citric acid (A), abscisic acid (B), gibberellic acid (C) and jasmonic acid (D).

usually observed in photocatalysis processes cannot be formed. Photoelectron capture dissociation is demonstrated by the negative ion of long chain fatty acid C16:0 at m/z 255 shown in Supplementary Figure 2A. This ion was generated through the capture of a tunneling electron by the charge deficient carbon atom of the carboxyl group. Resultant unpaired-electron subsequently directs the cleavage of α O-H bond (Supplementary Figure 2B). Localization of charge deficient atoms and prediction of electron-directed chemical bond cleavage can be achieved with DFT calculation.

Compared with general MALDI approach, there are no background peaks from bismuth cobalt zinc oxide in the low mass region by using LAET-based point electron emitting sources for *in situ* soft ionization. In addition, the thin film of bismuth cobalt zinc oxide particles provides a uniform distribution of matrix nanoparticles. These features make LAET an ideal imaging technique for displaying the distribution of different molecules. Supplementary Figure 3 represents the plot of absolute mass spectrometric intensities of molecular ion at m/z 209.1196 of jasmonic acid versus different quantities. It was found that absolute intensities of molecular ions are correlated well with quantities. These experimental results indicate that intensities of each pixel in a LAET mass spectrometric imaging should be able to reflect the quantities of analyzes in different locations. Then it is possible to compare ion distribution in different tissue sections. Supplementary Figure 4 shows that flavone derivatives are not present in the roots but fatty acid C16:0 is highly abundance in the same sections. However, it should be mentioned that ion suppression resulting from co-existing molecules still limits the application to absolute quantification. Other phytohormones and organic acids have also been studied. For all these compounds, tunneling electrons are captured by charge deficient carbon atoms of carbonyl groups and unpaired-electrons cause subsequent cleavage of α O-H bond. As an example, production of molecular ion at m/z 209 of representative jasmonic acid was shown in Supplementary Figure 5. In this approach, fragmentation of molecules is controllable because the energy of emitting electrons is adjustable by changing the voltage applied on the sample plate. At low energies such as 20 eV used for routine MALDI experiments, emitting electrons are not able to cause intra-molecular vibrational excitation because the de Broglie wavelength of emitting electrons does not match the typical bond length of organic molecules. Therefore, the possibility to generate non-specific fragmentation observed in SIMS can be decreased.

Actually LAET can work with two modes of fragmentation^{16,17}. In addition to the unpaired electron-directed chemical bond cleavages, CAD (collision activated dissociation) can also be complemented for more detailed structural specificities. Figure 1(A) is the MS spectrum of the leaf. By searching molecular masses against METLIN database, two dominant peaks at m/z 269.0453 and 285.0404 have been putatively identified as flavone

derivatives with three and four OH groups in benzoic rings respectively. Further MS/MS spectrum of the ion at m/z 269.0453 shown in Fig. 1(B) provides experimental evidences for the identification of this flavone derivative but the positions of two OH groups remain unknown. However, LAET can spontaneously generate fragment ions through electron-directed chemical bond cleavage without MS/MS experiments. The predictable fragmentation makes LAET an ideal tool for identification of small molecules. Figure 1(C) illustrates the production of the fragment ion at m/z 117.0340 and the possible positions of OH groups were indicated with red circles. Visualization of the distribution of these two flavone derivatives as well as the fragment ion at m/z 117.0340 was shown in Fig. 1(D). *Cayratia japonica* has been traditionally recognized as a Chinese medicinal herb. The presence of abundance flavone derivatives of this plant makes it useful to treat certain diseases²⁶. Figure 1(D) indicates that this kind of natural products distributes across the whole leaf.

In order to proof that laser activated electron tunneling (LAET) from semiconductor nanoparticles initiate the ionization process, a tape has been stuck to the back of the leaf. Figure 2(A) shows the averaged MS spectrum of the tape-blocked leaf and several strong peaks have been observed. The imaging at m/z 106.9742 shown in Fig. 2(B) reveals that no signal can be detected except very weak background molecules around the leaf, meaning LAET cannot occur on the surface of the tape. However, as shown in Fig. 2(C), even weaker molecules at m/z 168.9814 probably resulting from the ionization of the tape material can be observed in the area where the tape was stuck. These experimental results confirm that irradiation of ultraviolet laser on surfaces of semiconductor nanoparticles is essential to the generation of photoelectrons and subsequent electron-directed soft ionization of neutral molecules as well as chemical bond cleavages.

Imaging of organic acids and phytohormones in plant leaves with LAET. In addition to abundant flavone derivatives, other different ions have been detected with reasonable mass accuracy (Supplementary Table 1). Representative fatty acids, small organic acids and plant hormones were putatively identified by their masses (error < 35 ppm) and related fragment ions. No MS/MS experiments were performed for these endogenous metabolites because of their low abundance. The accuracy of detected molecular ions can be down to three decimals. Lower intensities of molecular ions usually result in decreased mass accuracy. Figure 3(A–D) shows the spatial distribution of fatty acids including C18:3, C18:2, C18:1 and C18:0. Other fatty acids have been shown in Supplementary Figure 6–21. The content of these fatty acids fluctuates across the whole section of the leaf. Among these, polyunsaturated long chain fatty acid C18:3 at m/z 277 shows relatively more uniform distribution while the others were found to be more abundant on the left side of the leaf. Uneven distribution of endogenous metabolites may result from nutritional differences, bias of sunlight, defenses or other physiological processes^{27–30}.

In addition to long chain fatty acids, some small organic acids have also been detected. Figure 4(A) shows the spatial distribution of citric acid. It is interesting to find that this acid accumulates more around the stem where the leaf was cut. Small organic acids have been found in many plants and juice of fruits^{31–34}. Tissue localization of these compounds is essential to investigate their versatile roles in every kind of physiological processes³⁵. Phytohormones constitute another subclass of endogenous metabolites in plants that are important for immobile plants to sense and respond to environmental stresses^{36–39}. Figure 4(B–D) shows different accumulation patterns for different phytohormones. The image of representative fragment ion of gibberellic acid (GA) was shown in Supplementary Figure 22. In general, these small signaling molecules are all unevenly distributed across the whole leaf. All of them were found to be more abundant in the left side of this leaf and around the stem where this leaf was cut. Among them, jasmonic acid (JA) and gibberellic acid (GA) were slightly more abundant in the middle of the left side. The interaction of salicylic acid (SA) and abscisic acid (ABA) has been reported in response to temperature changes. In plant cells, increased production of SA or ABA was considered as one of the consequences of temperature change senses and transduction of perceived signals⁴⁰. Meanwhile, interactive effects of JA and GA on induction of trichomes in *Arabidopsis* have also been reported^{41,42}.

Conclusion

Compared with other approaches for direct tissue analysis, LAET offers the opportunities for endogenous metabolites of plants to be ionized and dissociated from biological context without background peaks. With LAET method, delocalization of analytes caused by organic solvents in routine MALDI analysis is avoided because it is a solvent-free approach. The uniform surface of matrix nanoparticles simplifies the sample preparation process and enhances the spatial resolution as well as analytical reproducibility. It generates hot electrons *in situ* with adjustable energies for *in situ* soft ionization of biological molecules. Thus energetic fragmentations observed in high energy SIMS approach are avoided.

In summary, soft ionization of biological molecules on nanoparticles of bismuth cobalt zinc oxide is achievable. Atoms present in nanoparticles function as point electron emitting sources when laser activated electron tunneling occurs. Thermal electrons tunneling away from the surface can be captured by charge deficient atoms and unpaired electrons cause subsequent chemical bond cleavages. LAET provides a new and clean way for direct analysis of plant tissues.

References

- Slodzian, G., Daigne, B., Girard, F., Boust, F. & Hillion, F. Scanning secondary ion analytical microscopy with parallel detection. *Biol Cell* **74**, 43–50 (1992).
- Delcorte, A., Bour, J., Aubriet, F., Muller, J. F. & Bertrand, P. Sample metallization for performance improvement in desorption/ionization of kilodalton molecules: quantitative evaluation, imaging secondary ion MS, and laser ablation. *Anal. Chem.* **75**, 6875–6885 (2003).
- Cornett, D. S., Reyzer, M. L., Chaurand, P. & Caprioli, R. M. MALDI imaging mass spectrometry: molecular snapshots of biochemical systems. *Nat. Methods* **4**, 828–833 (2007).
- Li, Y., Shrestha, B. & Vertes, A. Atmospheric pressure infrared MALDI imaging mass spectrometry for plant metabolomics. *Anal. Chem.* **80**, 407–420 (2008).

5. Angel, P. M., Spraggins, J. M., Baldwin, H. S. & Caprioli, R. Enhanced sensitivity for high spatial resolution lipid analysis by negative ion mode matrix assisted laser desorption/ionization mass spectrometry. *Anal. Chem.* **84**, 1557–1564 (2012).
6. Takats, Z., Wiseman, J. M., Gologan, B. & Cooks, R. G. Mass spectrometry sampling under ambient conditions with desorption electrospray ionization. *Science* **306**, 471–473 (2004).
7. Ifa, D. R., Manicke, N. E., Dill, A. L. & Cooks, R. G. Latent fingerprint chemical imaging by mass spectrometry. *Science* **321**, 805 (2008).
8. Eberlin, L. S., Ifa, D. R., Wu, C. & Cooks, R. G. Three-dimensional visualization of mouse brain by lipid analysis using ambient ionization mass spectrometry. *Angew. Chem. Int. Ed.* **49**, 873–876 (2010).
9. Andersson, M., Groseclose, M. R., Deutch, A. Y. & Caprioli, R. M. Imaging mass spectrometry of proteins and peptides: 3D volume reconstruction. *Nat. Methods* **5**, 101–108 (2008).
10. Huh, W. K. *et al.* Global analysis of protein localization in budding yeast. *Nature* **425**, 686–691 (2003).
11. Thomas, A., Charbonneau, J. L., Fournaise, E. & Chaurand, P. Sublimation of new matrix candidates for high spatial resolution imaging mass spectrometry of lipids: enhanced information in both positive and negative polarities after 1,5-diaminonaphthalene deposition. *Anal. Chem.* **84**, 2048–2054 (2012).
12. Northen, T. R. *et al.* Clathrate nanostructures for mass spectrometry. *Nature* **449**, 1033–1036 (2007).
13. Woo, H. K., Northen, T., Yanes, O. & Siuzdak, G. Nanostructure-initiator mass spectrometry: a protocol for preparing and applying NIMS surfaces for high-sensitivity mass analysis. *Nat. Protoc.* **3**, 1341–1349 (2008).
14. Greving, M. P., Patti, G. J. & Siuzdak, G. Nanostructure-initiator mass spectrometry metabolite analysis and imaging. *Anal. Chem.* **83**, 2–7 (2011).
15. Zhong, H., Fu, J., Wang, X. & Zheng, S. Measurement of laser activated electron tunneling from semiconductor zinc oxide to adsorbed organic molecules by a matrix assisted laser desorption/ionization mass spectrometer. *Anal. Chim. Acta* **729**, 45–53 (2012).
16. Tang, X., Huang, L., Zhang, W. & Zhong, H. Chemical imaging of latent fingerprints by mass spectrometry based on laser activated electron tunneling. *Anal. Chem.* **87**, 2693–2701 (2015).
17. Tang, X., Huang, L., Zhang, W., Jiang, R. & Zhong, H. Photo-catalytic activities of plant hormones on semiconductor nanoparticles by laser-activated electron tunneling and emitting. *Sci. Rep.* **5**, 8893 (2015).
18. Watanabe, T., Kawasaki, H., Yonezawa, T. & Arakawa, R. Surface-assisted laser desorption/ionization mass spectrometry (SALDI-MS) of low molecular weight organic compounds and synthetic polymers using zinc oxide (ZnO) nanoparticles. *J. Mass Spectrom.* **43**, 1063–1071 (2008).
19. Lin, Y. S., Tsai, P. J., Weng, M. F. & Chen, Y. C. Affinity capture using vancomycin-bound magnetic nanoparticles for the MALDI-MS analysis of bacteria. *Anal. Chem.* **77**, 1753–1760 (2005).
20. Qiao, L. *et al.* Specific on-plate enrichment of phosphorylated peptides for direct MALDI-TOF MS analysis. *J. Proteome Res.* **6**, 4763–4769 (2007).
21. Lorkiewicz, P. & Yappert, M. C. Titania microparticles and nanoparticles as matrixes for *in vitro* and *in situ* analysis of small molecules by MALDI-MS. *Anal. Chem.* **81**, 6596–6603 (2009).
22. Chen, S. *et al.* Carbon nanodots as a matrix for the analysis of low-molecular-weight molecules in both positive- and negative-ion matrix-assisted laser desorption/ionization time-of-flight mass spectrometry and quantification of glucose and uric acid in real samples. *Anal. Chem.* **85**, 6646–6652 (2013).
23. Jackson, S. N. *et al.* Imaging of lipids in rat heart by MALDI-MS with silver nanoparticles. *Anal. Bioanal. Chem.* **406**, 1377–1386 (2014).
24. Stubiger, G., Wuczkowski, M., Bicker, W. & Belgacem, O. Nanoparticle-based detection of oxidized phospholipids by MALDI mass spectrometry: Nano-MALDI approach. *Anal. Chem.* **86**, 6401–6409 (2014).
25. Kailasa, S. K., D'souza, S. & Wu, H. F. Analytical application of nanoparticles in MALDI-MS for bioanalysis. *Bioanal.* **7**, 2265–2276 (2015).
26. Han, X. H. *et al.* Monoamine oxidase inhibitory components from *Cayratia japonica*. *Arch. Pharm. Res.* **30**, 13–17 (2007).
27. Shroff, R., Vergara, F., Muck, A., Svatos, A. & Gershenzon, J. Nonuniform distribution of glucosinolates in *Arabidopsis thaliana* leaves has important consequences for plant defense. *Proc. Natl. Acad. Sci. USA* **105**, 6196–6201 (2008).
28. Holscher, D. *et al.* Matrix-free UV-laser desorption/ionization (LDI) mass spectrometric imaging at the single-cell level: distribution of secondary metabolites of *Arabidopsis thaliana* and *Hypericum* species. *Plant J.* **60**, 907–918 (2009).
29. Hrazdina, G., Marx, G. A. & Hoch, H. C. Distribution of secondary plant metabolites and their biosynthetic enzymes in pea (*Pisum sativum* L.) leaves: anthocyanins and flavonol glycosides. *Plant Physiol.* **70**, 745–748 (1982).
30. Gutterman, Y. & Chauser-Volfson, E. Secondary phenol metabolites (SPhMs), distribution and content of some Aloe species, originated from arid zones of South Africa: A review. *Am. J. Food Technol.* **2**, 555–569 (2007).
31. Lynch, J. M. Effects of organic acids on the germination of seeds and growth of seedlings. *Plant Cell Environ.* **3**, 255–259 (2006).
32. Melino, V. J., Soole, K. L. & Ford, C. M. Ascorbate metabolism and the developmental demand for tartaric and oxalic acids in ripening grape berries. *BMC Plant Biol.* **9**, 145 (2009).
33. Mukherjee, M. *et al.* Ascorbic acid deficiency in *Arabidopsis* induces constitutive priming that is dependent on hydrogen peroxide, salicylic acid, and the NPR1 gene. *Mol. Plant Microbe Interact.* **23**, 340–351 (2010).
34. Sun, Y. L. & Hong, S. K. Effects of citric acid as an important component of the responses to saline and alkaline stress in the halophyte *Leymus chinensis* (Trin.). *Plant Growth Regul.* **64**, 129–139 (2011).
35. Fiehn, O. *et al.* Metabolite profiling for plant functional genomics. *Nat. Biotech.* **18**, 1157–1161 (2000).
36. Erb, M., Meldan, S. & Howe, G. A. Role of phytohormones in insect-specific plant reactions. *Trends Plant Sci.* **17**, 250–259 (2012).
37. Schmelz, E. A. *et al.* Simultaneous analysis of phytohormones, phytotoxins, and volatile organic compounds in plants. *Proc. Natl. Acad. Sci. USA* **100**, 10552–10557 (2003).
38. Lin, L. & Tan, R. X. Cross-kingdom actions of phytohormones: a functional scaffold exploration. *Chem. Rev.* **111**, 2734–2760 (2011).
39. Piotrowska-Niczyporuk, A., Bajguz, A., Zambrzycka, E. & Godlewska-Zylkiewicz, B. Phytohormones as regulators of heavy metal biosorption and toxicity in green alga *Chlorella vulgaris* (Chlorophyceae). *Plant Physiol. Biochem.* **52**, 52–65 (2012).
40. Penfield, S. Temperature perception and signal transduction in plants. *New Phytol.* **179**, 615–628 (2008).
41. Traw, M. B. & Bergelson, J. Interactive effects of jasmonic acid, salicylic acid, and gibberellin on induction of trichomes in *Arabidopsis*. *J. Am. Soc. Plant Biol.* **133**, 1367–1375 (2003).
42. Masoud, A. N., Doorenbos, N. J. & Quimby, M. W. Mississippi-grown *Cannabis sativa* L. IV: Effects of gibberellic acid and indoleacetic acid. *J. Pharm. Sci.* **62**, 316–318 (1973).

Acknowledgements

We greatly appreciate the support from National Natural Science Foundation of China (NSFC, 21175054, 31270876, 31370815, 21575046), Ministry of Science and Technology of the People's Republic of China (MSTC, 2014DFB30020), Program for Changjiang Scholars and Innovative Research Team in University (PCSIRT, no. IRT0953), Hubei Natural Science Foundation Council (HBNSFC, 2009CDA001), Research Funds of Central China Normal University from the Ministry of Education (120002040270, CCNU11G01007, CCNU11C01002) and the Research Platform of Hubei Province for Monitoring of Pesticide Residues and Agricultural Products Safety.

Author Contributions

L.H. and X.T. contributed equally to this work. They performed all experiments and repeated with each other. W.Z. and R.J. have been involved in the experiments. D.C. performed DFT calculation. J.Z. performed MS experiments on regular MALDI for comparison. H.Z. developed the concept, designed experiments, analyzed data and wrote the manuscript. All authors reviewed the manuscript.

Additional Information

Supplementary information accompanies this paper at <http://www.nature.com/srep>

Competing financial interests: The authors declare no competing financial interests.

How to cite this article: Huang, L. *et al.* Imaging of Endogenous Metabolites of Plant Leaves by Mass Spectrometry Based on Laser Activated Electron Tunneling. *Sci. Rep.* **6**, 24164; doi: 10.1038/srep24164 (2016).



This work is licensed under a Creative Commons Attribution 4.0 International License. The images or other third party material in this article are included in the article's Creative Commons license, unless indicated otherwise in the credit line; if the material is not included under the Creative Commons license, users will need to obtain permission from the license holder to reproduce the material. To view a copy of this license, visit <http://creativecommons.org/licenses/by/4.0/>